The Frequency Response of Acoustic Doppler Current Profilers

Spatiotemporal response and implications for tidal turbine site assessment

Romain U. G. Guion, Anna M. Young
Whittle Laboratory
University of Cambridge
Cambridge, United Kingdom
romain.guion@gmail.com, amy21@cam.ac.uk

***Abstract* – The lifespan of a tidal turbine is strongly affected by the unsteady loading it experiences, so knowledge of the mean flow speed is not sufficient: unsteadiness must also be quantified. One of the most common turbulence measurement devices in the marine environment is the Acoustic Doppler Current Profiler (ADCP). The variance of steady velocity measurements from ADCPs has been studied in detail, but very little attention has been given to the fundamental limits of ADCPs in terms of the frequencies and lengthscales that they can capture.**

In this paper, it is shown that the ADCP acts as a low-pass filter to eddies and that even optimistic calculations predict significant attenuation at lengthscales up to ten times the blade chord of a typical tidal turbine. For a typical 40 m deep channel wavelengths below 3-4 m are attenuated by 90% or more. Those eddies that are not filtered out are then subject to a distortion that will either amplify or attenuate the signal depending on the precise turbulence characteristics of the site in question. While this low-pass filtering may alter some global statistics by truncating the observed spectrum, it is most damaging when data is extracted for particular frequencies, as a turbine designer may do when assessing unsteady loading and fatigue life.

It is therefore recommended that high-resolution turbulence data, e.g. from a hotwire, is captured over part of the water column and that this is used to calibrate ADCP data.

Keywords— ADCP, response, spatiotemporal, filter, dispersion relationships, capture, turbulence, tidal, turbines, energy site.

I. NOMENCLATURE

Roman Letters

a	Fourier harmonic amplitude
b	beamwise velocity
d	scatterer diameter
E	energy density
f	frequency
F	filter (1 for no filtering, 0 for infinite filtering)
h	channel depth
I	turbulence intensity ($I_u = \sigma_u/\bar{u}$)
k	wave number
L	turbulent integral lengthscale
N	number of pings
s	density ratio between scatterers and fluid
S_k	Stokes number
T	sampling period
u,v,w	Streamwise/transverse/vertical velocity
x,y,z	Streamwise/transverse/vertical coordinate

Greek Letters

α	beam slant angle (from vertical)
β	scatterer phase lag
γ	anisotropy ratio corrected by beam angle
ε	turbulent kinetic energy dissipation rate
η	scatterer amplitude damping ratio
θ	beam spread angle
λ	wavelength
Λ	dispersion amplitude parameter
ν	kinematic viscosity
ρ	density
σ	velocity standard deviation $\sqrt{\overline{u'^2}}$
ϕ_o	phase lag between streamwise and vertical eddy components
ω	angular frequency

Subscripts/superscripts

$(.)'$	instantaneous fluctuation
$\overline{(.)}$	Mean
$\overline{(.)'^2}$	RMS
$\widehat{(.)}$	Fourier transform
c	cut-off
f	fluid
p	particle

II. INTRODUCTION

While tidal power is intermittent, it is predictable, and this sets it apart from many other renewable resources. There are, however, major technical challenges to overcome before tidal power generation becomes commercially viable – mainly related to reliability and cost. This paper focuses on tidal stream turbines, which are similar in design to wind turbines, are much more sensitive to velocity fluctuations due to the lower average flow speeds encountered and the higher density of water [1]. Tidal turbines therefore experience higher unsteady forces than wind turbines, and this in turn causes fatigue.

Accurate calculation of these unsteady forces is vital in order to avoid either premature failure or over-engineering, both of which add cost and hamper commercial viability [2]. It is thus essential for designers to have correct information about the flow at each tidal energy site – in terms of turbulence as well as the mean flow speed. This will become even more important as developers seek to deploy devices in ever-harsher locations.

This paper assesses the measurement limitations of the most widely-used device for tidal current measurements, the Acoustic Doppler Current Profiler (ADCP). ADCPs are often used in the seabed-mounted Janus configuration, which uses four transducers arranged as shown in Fig. 1. Each transducer emits a beam of acoustic waves, which are backscattered by particles in suspension. The Doppler shift of each reflected signal is used to calculate the beamwise velocity of each particle, and the time taken for the signals to return is used to divide them into 'bins' denoting different distances from the ADCP. By combining data from all four beams, the streamwise, transverse and vertical velocity components can be calculated in each depth bin, and thus a 3D flow profile can be produced for the whole height of the channel.

The reliability of steady ADCP data is well-known, and the trade-offs between different performance metrics have been studied in detail – ranges of hundreds of metres can be achieved but this is at the expense of standard deviation and spatial resolution [3].

Improved technology and advanced post-processing techniques have enabled the use of ADCPs to be extended to provide an assessment of turbulence statistics [4]. Until now, however, very little attention has been given to the fundamental limits to the frequencies and lengthscales that ADCPs can capture. The little work that has been carried out suggests major issues in this respect.

Experiments by Nystrom et al. [5] found errors from 44% to 94% in turbulence intensity derived from ADCP data. On the theoretical side, Theriault [6,7] provided the first analysis, which was built upon by Gargett et al. [8,9], who focused on inter-beam information loss. They showed that a four-beam ADCP will give inaccurate data in the presence of anisotropic turbulence or when there are phase differences between the components of eddies.

Despite evidence that there are severe limitations to an ADCP's ability to capture turbulent flow structures, they are being used to analyse the frequency content of flows. Inaccuracies from these calculations could lead to misleading choices of tidal energy sites or poor estimates of fatigue life, particularly if errors arise away from the universal high-frequency range. Some researchers are also using instantaneous ADCP velocity profiles (u'and w') in an attempt to generate realistic coherent inflows for simulations [10,11].

To the authors' knowledge, no systematic study has been carried out of the capability of an ADCP to capture turbulent structures in the frequency range relevant to tidal turbines. This paper provides a conservative assessment of the unsteady response of an ADCP, and finds that the ADCP acts as a low-pass filter to turbulent structures. The intensity of this filter increases quickly with depth, with up to half the energy being lost by the top of a typical channel.

In the first part of this paper, the range of frequencies that affect a tidal turbine is discussed. After this, filters

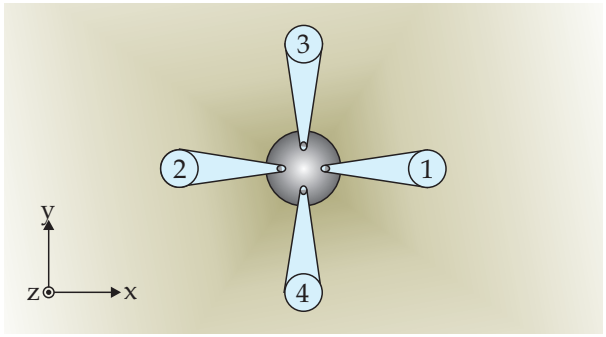

(a) Top view.

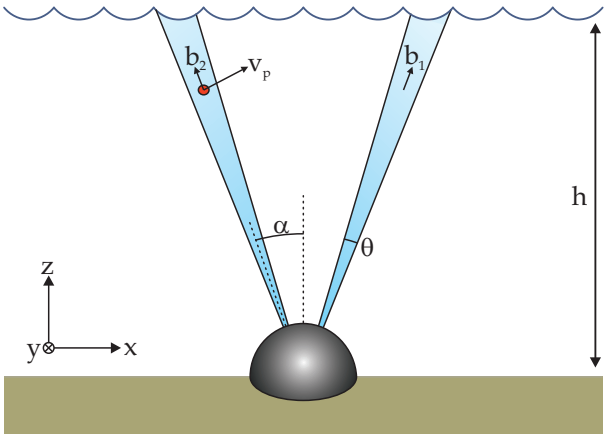

(b) Transverse view.

Fig. 1 - Four-beam ADCP in the Janus configuration.

representing the spatio-temporal response of an ADCP are defined. Next, dispersion relations are developed to assess where realistic eddies lie on these spatio-temporal diagrams. The filters are then used to assess cut-off frequencies and the proportion of energy captured with depth. Finally, guidance is provided for the use of unsteady data from ADCPs in tidal turbine design.

III. Frequencies Relevant to Tidal Turbines

The mechanical stresses on a turbine arise from steady and unsteady loads. The former depend on the average flow speed, while the latter are related to velocity fluctuations, and it is these unsteady loads that cause fatigue. While some velocity fluctuations (e.g. those due to the rotation of the blade through the channel boundary layer) are well-known, there are other, less predictable, sources of unsteady flow: turbulence, waves, large-scale structures generated by local bathymetry, and the wakes of other turbines. Many of these vary from one site to another, so accurate local data is vital.

The most damaging lengthscales will depend on the exact shape of the S-N curve of the materials used. Furthermore, the hydrodynamic response of the turbine to fluctuations (and thus the stress on the blade) does not only depend on the amplitude of the fluctuations in the

streamwise direction, but also on the vertical and transverse eddies.

As a rule of thumb, structures that are much smaller than the blade chord (typically 1.5 m) are unlikely to cause significant global thrust and torque variation [12]. Very small eddies can be predicted from standard turbulence theory, as they are unaffected by local bathymetry. This means that it is not necessary to measure eddies shorter than about 1 m.

For the upper bound, the maximum integral eddy lengthscale in a 40 m deep channel is about 35 m. However Thomson et al. [13] argue that the very large eddies may not be the largest contributors to turbine fatigue, and suggest relevant eddies are between about 1 and 10 m. These larger disturbances are also not amenable to theoretical prediction because they are generated in part by the local bathymetry [2].

It is therefore the case that eddies between 1 and 35 m must be measured accurately at each site, because they are too large to be predicted by turbulence theory, and they are also large enough to affect turbine loading.

IV. The ADCP as a Low-Pass Filter

An ADCP can be thought of as acting as a low-pass filter to turbulent flow structures. There are several sources of filtering, and the overall response is the product of the individual filters because the process is sequential. Broadly speaking, the filters can be split in to two groups:

1. **Intra-beam** (i.e. information loss within one beam).
2. **Inter-beam** (i.e. information loss due to combining data from different beams).

Intra-beam filtering sets an upper limit on the information that can be reconstructed from ADCP data, as it is independent of data analysis technique or flow characteristics.

Inter-beam filtering is the error generated when data from different beams is combined. The errors introduced at this stage depend on the type of turbulence statistic being generated – e.g. the assessment of the instantaneous 3D velocity components requires an assumption of instantaneous horizontal homogeneity, while the evaluation of the Reynolds stress simply requires that the flow is statistically homogeneous.

In this paper, the effect of sample rate is not considered. Typical ADCPs have sample rates up to 1 Hz, giving a Nyquist cut-off frequency of 0.5 Hz, and creating a practical frequency limit for standard ADCP data.

Intra- and inter-beam filtering will now be discussed in turn.

V. Intra-Beam Filtering

Intra-beam filtering is found to be the product of three filters. First, the damping due to scatterering particles failing to follow the flow perfectly. Second, filtering due to the spatial averaging over the volume of each beam. Third, filtering as a consequence of averaging over several pings. These filters will now be developed in turn before their combined effect is discussed.

A. Scatterers following the flow

Like other Doppler devices, ADCPs do not measure the speed of water directly, but instead capture the speed of suspended scatterers. It is therefore important to know how closely these scattering particles follow the flow.

The motion of a spherical particle in a fluid can be modeled by the Basset-Boussinesq Ossen equation[1]. The equation was studied quantitatively for the first time by Tchen [14], and the harmonic response was derived by Hinze [15], using Fourier integrals:

$$U_f = \int_0^\infty [a_1 \cos(\omega t) + a_2 \sin(\omega t)] d\omega$$

$$U_p = \int_0^\infty \eta [a_1 \cos(\omega t + \beta) + a_2 \sin(\omega t + \beta)] d\omega$$

where U_f and U_p are the speed of the fluid and particle, respectively. It can be seen that the particle moves at the same frequency, but with a different amplitude and phase to the flow (attenuated by a factor of η and lagging by β). An analytical solution commonly used in Laser-Doppler Anemometry [16] is that of Helmfelt & Mockros [17]:

$$\eta = \sqrt{(1 + c_1)^2 + c_2^2}$$

$$\beta = \tan^{-1}\left(\frac{c_2}{1 + c_1}\right)$$

where c_1 and c_2 are functions of the Stokes number, $S_k = \sqrt{\frac{\nu}{\omega\, d^2}}$, and the density ratio, $s = \rho_p/\rho_f$:

$$c_1 = \frac{\left[1 + \frac{9}{\sqrt{2}\left(s + \frac{1}{2}\right)} S_k\right]\left[\frac{1 - s}{s + \frac{1}{2}}\right]}{\frac{81}{\left(s + \frac{1}{2}\right)^2}\left[2S_k^2 + \frac{S_k}{\sqrt{2}}\right]^2 + \left[1 + \frac{9}{\sqrt{2}\left(s + \frac{1}{2}\right)} S_k\right]^2}$$

$$c_2 = \frac{\frac{9(1 - s)}{\left(s + \frac{1}{2}\right)^2}\left[2S_k^2 + \frac{S_k}{\sqrt{2}}\right]}{\frac{81}{\left(s + \frac{1}{2}\right)^2}\left[2S_k^2 + \frac{S_k}{\sqrt{2}}\right]^2 + \left[1 + \frac{9}{\sqrt{2}\left(s + \frac{1}{2}\right)} S_k\right]^2}$$

The amplitude of attenuation, η, is mainly controlled by the relative density of the particle, s. Therefore better flow-tracking behavior is expected from organic particles, such as plankton (which are mainly water), than heavier mineral particles, such as sand. In addition, small Stokes numbers (high frequencies or large particles) give the most significant drop in amplitude. This is shown on Fig. 2, which is a plot of attenuation against eddy frequency. Three different particle sizes and density ratios are modeled, corresponding to large and small mineral particles (black and blue lines respectively) and plankton (red line).

[1] Note: there will be additional errors in the vertical velocity if the particle is not neutrally buoyant

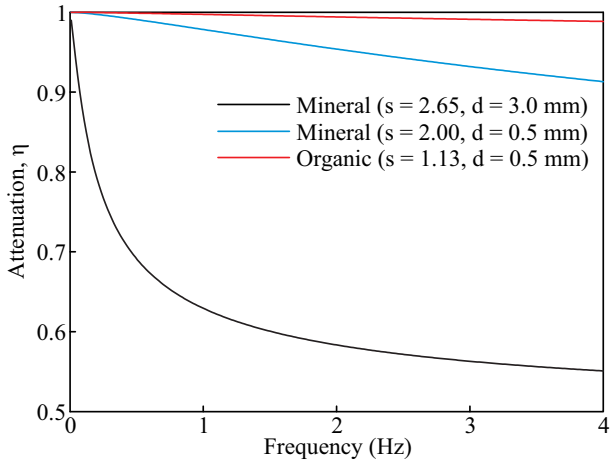

Fig. 2 - Amplitude attenuation of scatterers against frequency for three different particles.

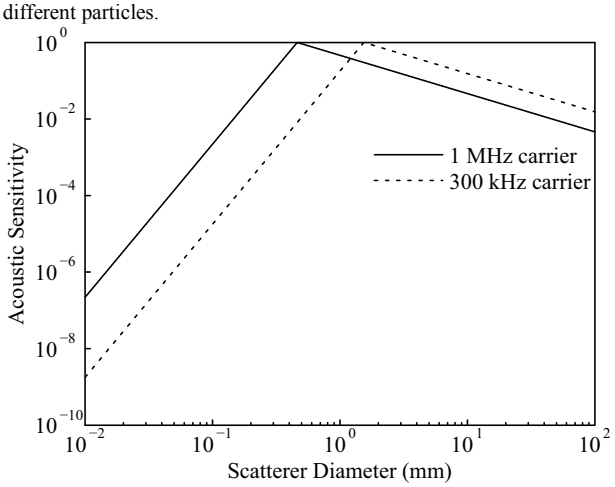

Fig. 3 - Acoustic sensitivity vs. scatterer diameter, for two carrier frequencies. Based on Lohrmann [4].

With a flow oscillating at 2.6 Hz (which corresponds to streamwise eddies with 1 m wavelength), mineral particles will have a speed 5-40% lower than that of water, depending and their size, while organic scatters will have an amplitude error closer to 1%.

At high frequencies, another source of error becomes important; variations in phase lag, β, between different scatterers will mean that they are out of phase. An ADCP averages the velocity of all the scatterers in a given bin, so that two scatterers going at the same speed but in opposite directions will cancel each other out, leading to a measurement of 0. This attenuation is not constant, but will have maxima at a series of frequencies depending on the density and size of each particle class present. As the amplitude of this filter is extremely site dependant, it is not included in the general results shown here.

At this point it is necessary to ask which particles will be the main contributors to scattering. The answer depends not only on the distribution of particles in the sea, but also on the scattering properties of these particles at the ADCP carrier wavelength. The peak acoustic sensitivity is when the perimeter of the particle is equal to the carrier wavelength. The acoustic sensitivity of particles in this size range is difficult to study, as it depends on the acoustic properties of the scatterers themselves [18].

Given that the speed of sound in the sea is about 1450 m/s, and carrier frequencies of ADCPs range from 300 kHz to 1200 kHz, the peak sensitivity is for particle diameters of about 0.5-1.5 mm. This is shown in Fig. 3, which is a plot of typical acoustic sensitivity for the relevant size range. This means that the data collected will be heavily biased towards particles of these radii. To correct this, site-dependant calibration would be necessary, which would involve measuring sampled water at different frequencies.

B. Spatial averaging

Each beam captures the particle speed along its axis (the 'beamwise' direction), and therefore contains a component of the vertical velocity as well as either a component of the streamwise or transverse speed. The accuracy of the velocity in the beamwise direction is affected by the vertical resolution within the beam. This finite resolution acts as a filter to the vertical and horizontal velocity components. The key difference is that the amount of information lost in the vertical direction depends on the size of the bins, Δr, but the horizontal filtering is independent of bin size. These two filters are now considered in turn.

1) Vertical resolution

Spatial averaging inside each beam is an inevitable feature of ADCPs. From the geometry of a bin (shown on Fig. 4), the vertical resolution is:

$$\Delta z = z\theta \tan(\alpha) + \Delta r \cos(\alpha)$$

where Δr is the radial 'bin' size, θ is the beam spread angle and α is the beam angle from the vertical.

Δz depends on the radial resolution, Δr, which depends on the signal processing method employed. It is interesting to note that when $\Delta r \to 0$the vertical resolution does not reduce to zero, but to $z\,\theta \tan(\alpha)$. Using typical values for both an ADCP and a tidal channel (see Table 1), when Δr = 0, Δz = 0.4 m. This is the lower bound for vertical resolution, regardless of bin size.

2) Horizontal filter

Fig. 4 also shows the horizontal cross section of the beam, which is an ellipse with axes $z\theta/\cos(\alpha)$ and $z\theta/\cos^2(\alpha)$. For simplicity, only the axis producing the largest loss of information will be considered, i.e. $\Delta x = z\theta/\cos^2(\alpha)$, which is approximately 0.6 m at 20 m depth.

The effect of averaging over the horizontal cross section can be estimated by assuming a uniform averaging over the bin and zero elsewhere. In the spatial domain, this is a window, $F_{intra}(x)$, as shown on Fig. 5. Shifting to the spectral domain, the Fourier transform of a rectangular function is a sinc function. This is a low-pass filter:

$$\hat{F}_{intra}(k_x) = sinc(k_x\,\Delta x)$$

An equivalent filter applies in the transverse direction. The cut-off frequency of this filter is considered to be the first zero of $\hat{F}_{intra}$, which is $k_c = \frac{\pi}{\Delta x}$. This corresponds to

Table 1 – Base case constants.

Name	Symbol	Base case
ADCP beam inclination angle (°)	α	20
ADCP beam width angle (°)	θ	1.5
Average flow velocity at mid depth	$\bar{u}$	2.6
Kinematic viscosity (m^2/s)	ν	10^{-6}
Turbulence intensity (streamwise)	I_u	10%
Channel depth (m)	h	40
Upper position of blade tip (m)	z	30
Number of pings averaged	$2N+1$	11
Relative density of scatterers	s	2
Size of scatterers (m)	d_p	$5 * 10^{-4}$
Phase interaction of scatterers	n/a	Excluded

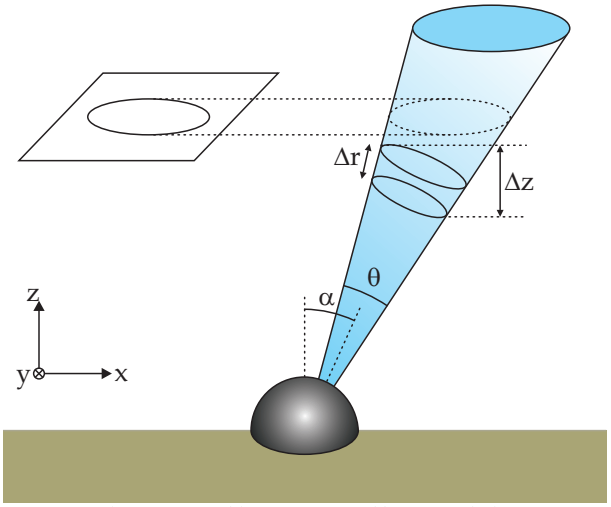

Fig. 4 - ADCP bin geometry and beam resolution.

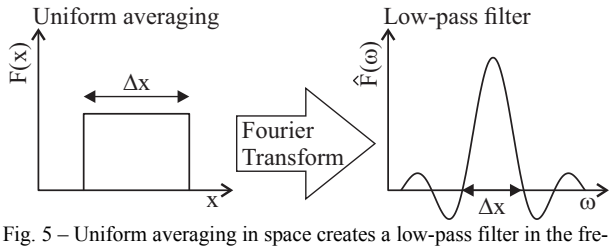

Fig. 5 – Uniform averaging in space creates a low-pass filter in the frequency domain.

a wavelength of 3.6 m for a typical ADCP. This low-pass filtering means all wavenumbers above the cut-off wavenumber are strongly attenuated. For first-generation, narrowband, ADCPs, this low-pass filtering was advantageous as it reduced aliasing in both time and space. However, aliasing is not the limiting factor of modern ADCPs as they have higher sampling rates (pulse coding has enabled intra-pair superposition).

C. *Averaging over several pings*

Modern broadband ADCPs achieve excellent single-ping velocity variance. However, older systems or demanding environments push users to collect data over several pings to reduce the velocity variance to an acceptable level. This subsection shows the consequences of ping averaging.

Assuming that the mean flow speed is constant over the averaging period and 2N+1 samples are taken at uniform time intervals, T (centred on x=y=0), the streamwise and transverse velocity, $\tilde{u}$ and $\tilde{v}$, will be:

$$\tilde{u} = \frac{u}{2N+1}\sum_{i=-N}^{N}\cos([\omega - k_x\bar{u}]T\,i)\ , \quad \tilde{v} = \frac{v}{2N+1}\sum_{i=-N}^{N}\cos(\omega\,T\,i)$$

In the frequency domain, the sum is geometric, so that:

$$\hat{F}_{avg,x}(\omega,k_x) = \frac{1}{2N+1}\frac{\sin\left([\omega - k_x\bar{u}]\,T\frac{2N+1}{2}\right)}{\sin\left([\omega - k_x\bar{u}]\frac{T}{2}\right)}$$

$$\hat{F}_{avg,y}(\omega) = \frac{1}{2N+1}\frac{\sin\left(\omega\,T\frac{2N+1}{2}\right)}{\sin\left(\omega\frac{T}{2}\right)}$$

In the streamwise direction, frozen eddies (where $\omega = k_x\bar{u}$) will not be attenuated at all. All sweeping and straining eddies (see Section VIII), and those in the transverse direction, will be attenuated periodically (at every frequency that is a multiple of the averaging period).

D. *Combined single-beam filter*

The filters described above can be multiplied together to create an overall filter for a single beam:

$$\hat{F}_{beam}(\omega,k) = \hat{F}_{particle}(\omega)\hat{F}_{intra}(k)\hat{F}_{avg}(\omega,k)$$

Considering the 'base case' given in Table 1, the frequencies and wavelengths captured by a single beam in a typical channel can be found. This is shown in Fig. 6, which is a contour plot of filter attenuation over the range of frequencies and wavelengths of interest. The white region shows areas where the attenuation is greater than 10 dB. Fig. 6(a) shows the streamwise filter while Fig. 6(b) shows the transverse filter. It can be seen that there is more than 90% attenuation of frequencies above 1 Hz in the streamwise direction and 0.3 Hz in the transverse direction. Wavelengths shorter than 4 m in either direction are attenuated by at least 90%. Above the initial cutoff, there are small areas where more than 10% of the signal is retained (for example, around 0.7 Hz in the transverse direction). The filter repeats periodically, so that frequencies between 3 and 4 Hz are also captured by the beam.

Not all combinations of wavelength and frequency are physically reasonable, so only certain areas on Fig. 6 represent realistic eddies. To address this, dispersion relations will be developed in Section VIII.

VI. Inter-beam filtering

Inter-beam filtering is extremely sensitive to the type of turbulence present in the channel, and to the data extracted. It is nonetheless useful to consider the effect of this filter in a general manner.

With the exception of the variance method (used to estimate Reynolds' stress), most turbulence statistics are found by combining instantaneous beamwise velocity estimates, b_i, to find the Cartesian velocity components.

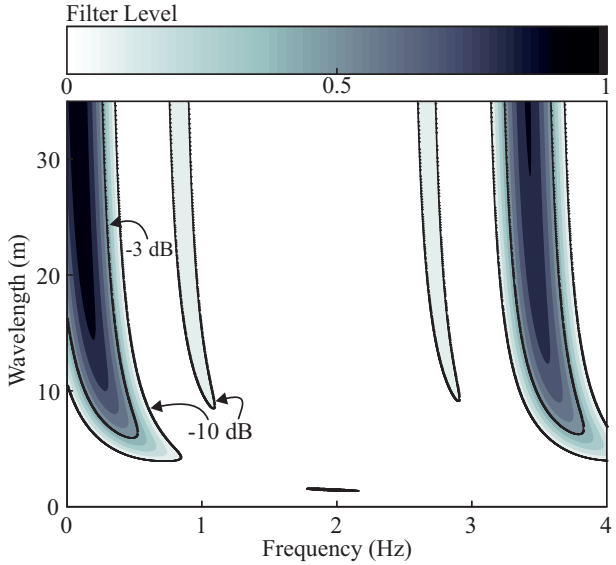

(a) Streamwise filter.

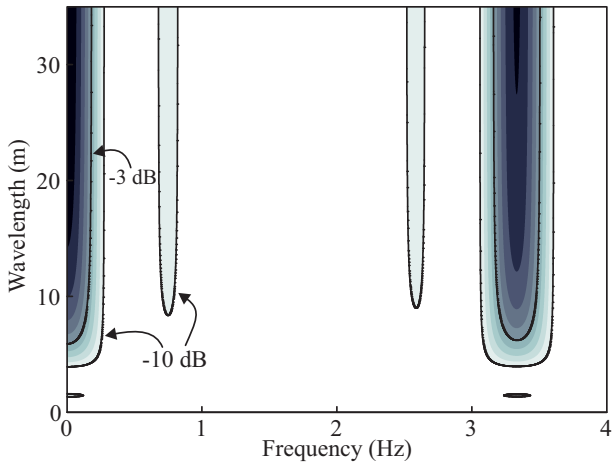

(b) Transverse filter.

Fig. 6: Overall single-beam filter: Contours of Filter Level for wavelength-frequency range relevant to turbines.

For instance, the streamwise velocity component, u, is found by combining b_1 and b_2 (see Fig. 1(a)):

$$\frac{b_1 - b_2}{2} = \frac{u(x + z\tan\alpha) + u(x - z\,tan\alpha)}{2} + \frac{w(x + z\,tan\alpha) - w(x - z\,tan\alpha)}{2}$$

Any changes in u or w between the two beams will affect the estimation of u. The size of this effect depends on the variation in velocity from one beam to another. Theriault [7] proposed a simple way to model this by assuming a uniform vertical velocity, w, so that only changes in streamwise velocity are considered. This results in a periodic filter that attenuates a large part of the wavenumber spectrum:

$$\hat{F}_{inter}^{Theriault}(k) = \cos\left(kz\tan(\alpha)\right)$$

It can be seen that the filter is a function of both wavenumber and depth, so the most strongly-attenuated frequencies change with depth. For instance, if z = 20 m and $\alpha = 20^o$, the zero wavelengths ($\lambda_0 = \frac{2\pi}{k}$) are 29 m, 9.7 m, 5.8 m, 4.2 m, 3.2 m, etc. At these wavelengths, the signal is completely attenuated.

Gargett et al. [8,9] extended this work, and showed that anisotropy, along with any phase difference between the horizontal and vertical components of an eddy, would have important effects on the filtering of flow structures, and could lead to amplification as well as attenuation. They called the phase difference ϕ_o so that:

$$u' = \sigma_u e^{ik_x x}$$
$$w' = \sigma_w e^{i(k_x x + \phi_0)}$$

Gargett et al. then defined an alternative anisotropy ratio, $\gamma = \frac{\sigma_w}{\sigma_u} * cot(\alpha)$, so that the filter becomes:

$$\hat{F}_{inter}^{Gargett}(k_x) = \sqrt{\cos^2(k_x z\ tan\alpha) + \gamma^2 \sin^2(k_x z\ tan\alpha) - \gamma sin(\phi_0)\sin(2k_x z\ tan\alpha)}$$

This filter reduces to Theriault's case when $\phi_0 = 0$. Fig. 7 shows the effects on the filter of changes in phase difference (Fig. 7(a)) and anisotropy (Fig. 7(b)), as functions of $kz\ tan\alpha$. Expressed in this way, the functions are periodic and so only the first period is shown in Fig. 7. Convective eddies typically have anisotropy $\frac{\sigma_w}{\sigma_u} \sim 0.56$ (giving $\gamma = 1.54$) [2], and do not exhibit strong phase relationships.

The lines representing these eddies are shown in red on Fig. 7. It can be seen that, for these typical eddies, there is up to 50% amplification, but no attenuation. However, Gargett et al. [8,9] found that wind- and storm-driven turbulent flows, such as Langmuir Supercells, have quasi-deterministic phase relationships ($\phi_o \approx 90^o$ or 180^o). An example of this is shown on Fig. 7(b) in blue[2], and it can be seen that there is total attenuation at some frequencies as well as almost doubling of the amplitude at others. This means that storm conditions and straining eddies are likely to be measured incorrectly by ADCPs.

Fig. 8 shows the same filter expressed as a function of wavelength for z = 20 m and $\alpha = 20^o$. It can be seen that both attenuation and amplification can be expected within the range of interest to tidal turbine designers, and it is not until the wavelength is greater than 100 m that the filter tends towards unity. This means that an ADCP will skew the frequency spectrum by attenuating some harmonics but amplifying others.

VII. Breakdown of the Filter

To give an idea of the relative importance of the filters presented above, a breakdown of the filters as applied to frozen turbulence is shown in Fig. 9. A filter of zero dB would mean perfect transmission of all information. As each filter is applied, the information is skewed, and the final filter is represented by the black line, which ranges from 2 dB amplification to >10 dB attenuation depending

[2] Note: For a Langmuir Supercell, ϕ_0 depends on the relative direction of the wind and current, and will change with depth. $\phi_o \approx 90^o$ is shown as an example.

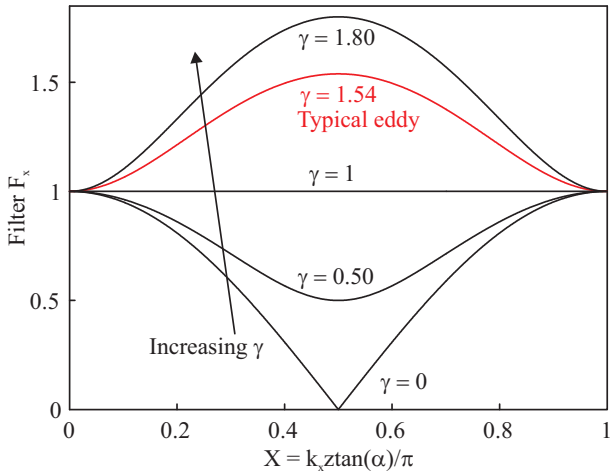

(a) Effect of Anisotropy ratio with $\phi_0 = 0$.

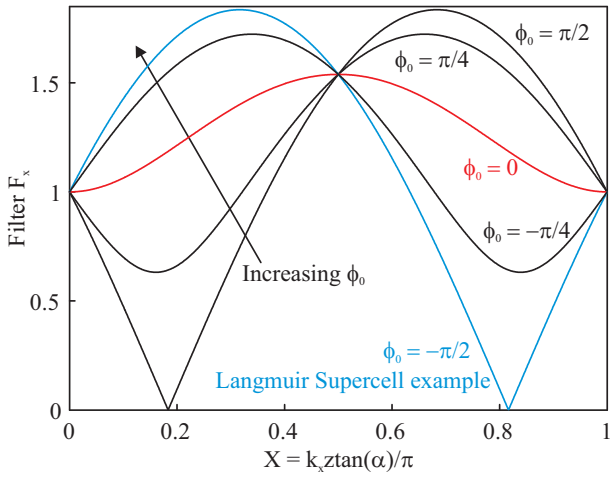

(b) Effect of phase difference with $\gamma = 1.54$.

Fig. 7 - Inter-beam filter based on Gargett et al. [9]. (X = 0.5 corresponds to a wavelength of 30 m when z = 20 m).

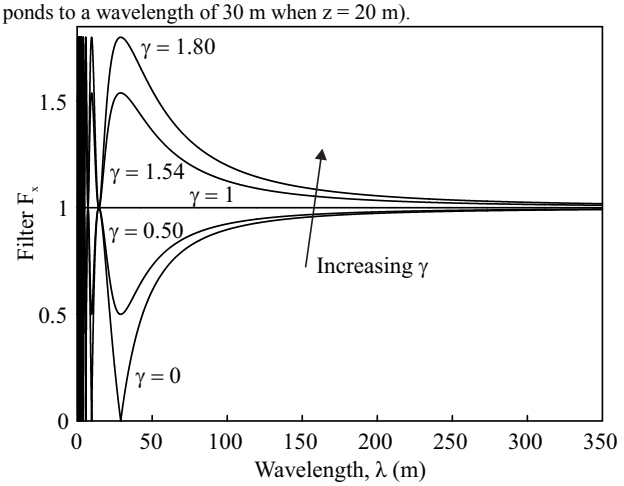

Fig. 8 - Inter-beam filter against wavelength for different anisotropy ratios ($\phi_0 = 0$). Based on Gargett et al. [9].

on the wavelength in question. This black line represents the final signal from the ADCP.

In Fig. 9(a), the tracking filter (black area) is almost non-existent, because the scatterers have 0.5 mm diameter, which corresponds to the peak sensitivity of a 1 MHz ADCP. For lower carrying frequencies, or in the presence of a high concentration of larger particles, flow tracking errors are much more significant, as shown in Fig. 9(b) (3 mm particles). The spatial average filtering (blue area) is more powerful, and leads to a -3 dB cutoff of about 6 m and a -10 dB cutoff of almost 4 m in both cases. Without inter-beam filtering, the filter would follow this blue area, with very little attenuation of wavelengths over 6 m (as shown in Fig. 6).

The final filters shown in Fig. 9 are inter-beam filters (red). Fig. 9(a) shows a Langmuir Supercell-like disturbance ($\phi_o = 90^o$), while Fig. 9(b) shows a typical convective eddy. Once these filters are included there is amplification of some frequencies. This shows that, with the inter-beam filtering included, parts of the spectrum may be lost, while other parts are amplified.

There are multiple additional sources of error not in Fig. 9, for example: limited sample rates, imperfect data processing, noise (including Doppler noise), and averaging over multiple pings.

The qualitative analysis above shows that the construction of turbulent flow data from several ADCP beams can be dangerous without good knowledge of the flow, because measurements could be over- or under-estimates, and in the worst case the errors could be orders of magnitude. Suggestions for mitigating errors will be made in Section X.

VIII. Effect of Different Dispersion Relations

Fig. 6 shows the operating windows of an ADCP, but not all points in the f-ω space are physically plausible in a realistic flow, as frequency and wavelength are linked. The aim of this section is to develop dispersion relations to model typical eddies in a tidal channel.

Any dispersion relation can be decomposed into an advection component and an additional part due to the evolution of turbulence:

$$\omega = k_{adv}\bar{u} + \omega_{turb}$$

When $\omega_{turb} = 0$, this is frozen flow as described by Taylor [19] and used in Sections VI and VII. Non-linear interactions between different flow structures mean that eddies change with time. Dispersion relations for the two most common changes (sweeping and straining) were defined by Fung et al. [20][3]:

1. **Sweeping** of small eddies by larger eddies. In this case, $\omega_{turb} = \Lambda_D k \overline{u'^2}$.
2. **Straining**: rotation of large eddies due to vortex stretching/compression (Kolmogorov eddy turnover). Here, $\omega_{turb} = \Lambda_D \sqrt{[k^3 E(k)]} \approx \Lambda_D \epsilon^{1/3} k^{2/3}$.

In both cases, Λ_D is a dispersion amplitude parameter, usually 1 [21]. The boundary between sweeping and

[3] More complex turbulence (e.g. from wind/waves) will not follow this description.

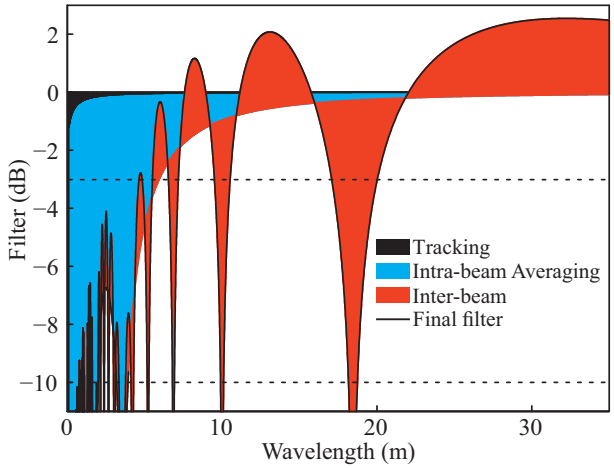

(a) Typical mineral particle (s = 2, d = 0.5 mm), Langmuir Supercell (γ=1.54, $\Phi_0 = 90^o$)

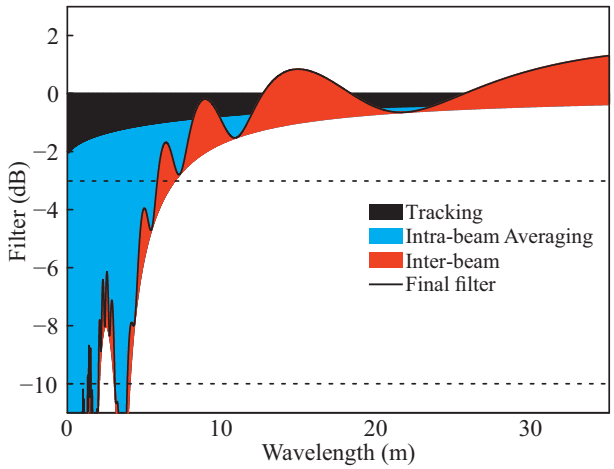

(b) Large mineral particle (s = 2, d = 3 mm) Convective eddy (γ=1.54, $\Phi_0 = 0^o$)

Fig. 9 – Filter integrated along frozen-flow line at z=30m, and broken down by filter type for two different scenarios.

straining is site-dependant, although it is typically around a wavelength of 22 m in a tidal channel.

These dispersion relations can now be used to show where typical eddies lie. These are denoted by the red lines plot ted on Fig. 10, which is a large-scale version of the low-frequency part of Fig. 6 (again, white denotes greater than 10 dB attenuation).

In the streamwise direction (Fig. 10(a)), it can be seen that both sweeping and straining eddies behave very similarly to the frozen flow case. In the transverse direction (Fig. 10(b)), however, the sweeping and straining eddies follow different paths and so the 4 m wavelength cut-off corresponds to a frequency of anywhere from 0.02 Hz (straining) to 0.6 Hz (sweeping). (There is no bulk flow in this direction so the frozen advection case does not occur.)

As discussed in Section V. C, frozen eddies are unaffected by averaging over multiple pings, but any sweeping or straining flow will be attenuated by averaging.

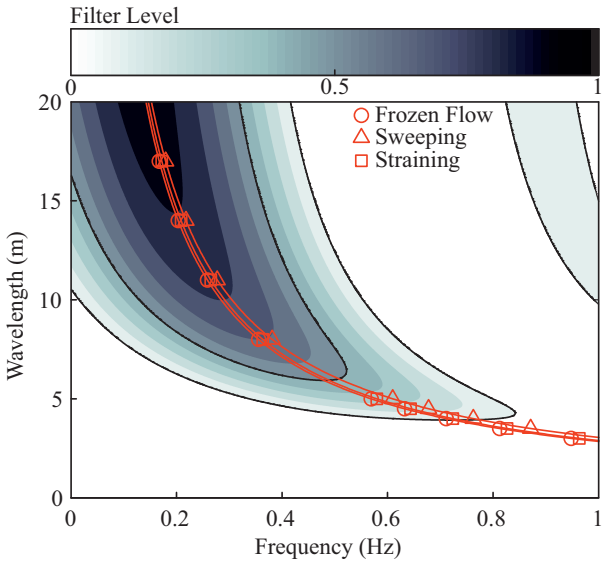

(a) Streamwise filter.

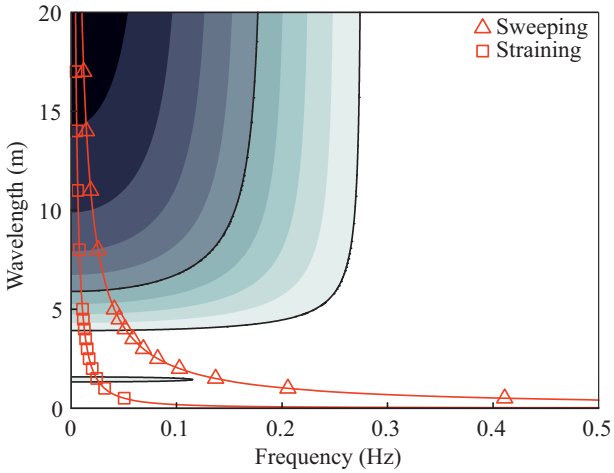

(b) Transverse filter.

Fig. 10– ADCP attenuation of flow field (contour plot) compared to dispersion relations for eddy motion (red).

IX. Influence of Depth on Energy Captured

Most of the filters developed above are depth dependent. This is because the beams become further apart, and the beam width increases, so both intra- and inter-beam filtering becomes broader further from the ADCP. In this Section, the effect of depth on both the -10 dB cut-off frequency and on the proportion of energy captured will be discussed.

A. Influence of depth on amplitude cutoff

Fig. 11 shows the depth-dependence of the data losses. The dark grey areas show the operating windows of the ADCP, bounded by the -10 dB cut-off (i.e. in the white areas, there is greater than 90% attenuation). In Fig. 11(a), only the intra-beam effects have been included. The -10

dB cut-off increases almost linearly with depth because of the local linearity of sinc close to its zeros. This means

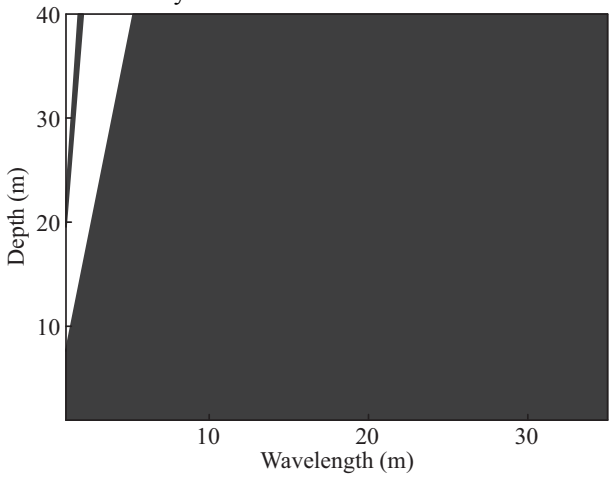

(a) Single-beam filter.

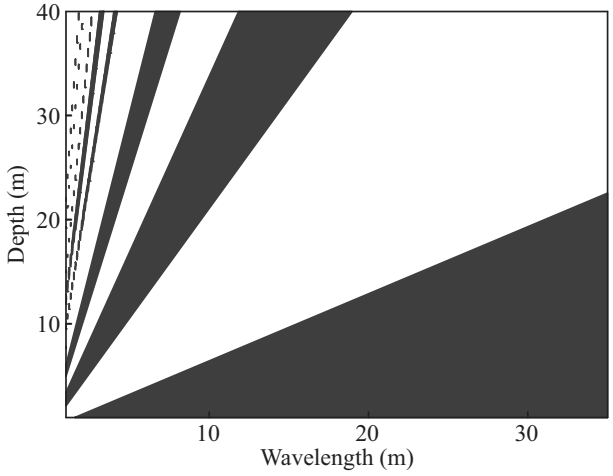

(b) With inter-beam filtering ($\gamma = 0$, $\phi_o = 0$).

Fig. 11 – -10 dB cutoff as a function of depth and wavelength for frozen eddies (white areas have >90% attenuation).

that, while eddies as small as 1 m may be captured very close to the seabed, the cutoff has increased to almost 6 m by the top of the water column. In Fig. 11(b), inter-beam filtering has been included (with no anisotropy or phase difference), and it can be seen that the operating windows are now much more sparse, with large parts of the spectrum excluded.

B. Influence of depth on energy captured

The proportion of the energy observable by ADCPs, before any data processing is shown on Fig. 12(a), where the energy captured at each depth has been found by integrating the filter shown in Fig. 11. Without inter-beam filtering (base case), ADCPs can capture up to about 92 % of the spectrum at the top of the channel and up to 98% at the bottom. For more complex eddies, where inter-beam filtering is much more significant the energy captured can drop to 60-80%.

As already discussed, not all of the energy in the spectrum will affect the fatigue of a tidal turbine. If only

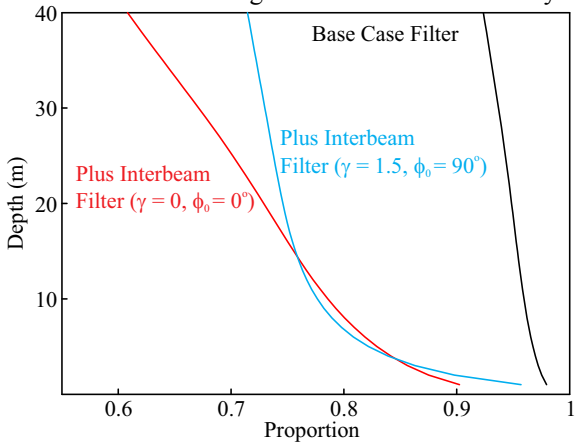

(a) Proportion of total energy spectrum with three different filters.

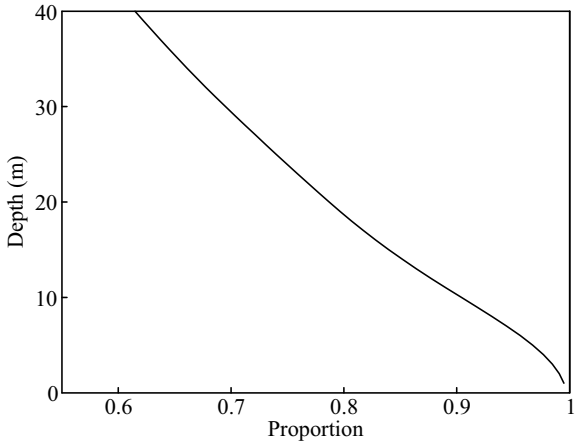

(b) Proportion of energy in 1-35 m range, base case filter.

Fig. 12 – Proportion of turbulent energy captured by an ADCP as a function of depth.

wavelengths in the 1-35 m range are considered, ADCPs capture only 65% of the energy affecting the turbine by the tip height, even when only the base case intra-beam filtering is considered (Fig. *12* (b)).

X. Implications for Tidal Site Assessment

The results shown above make it clear that turbulent statistics calculated from ADCP data will not capture the whole spectrum. The filtering processes mean that some frequencies are attenuated completely, while others will be amplified. This means that the turbulence spectrum will be skewed by an ADCP.

As mentioned above, the implications of this for practical use will depend on the statistics produced. For example, if each beam can be considered separately, as is the case when calculating Reynolds' stress, it is possible to correct for the missing energy content.

There are ways to mitigate some of these errors. For example, if the water is sampled to find the distribution of particles, the damping described in Section V. A can be

corrected. It would also be advantageous to have knowledge of the weather at the time (to correct for any large wind/wave-induced structures) and the anisotropy of the flow.

Perhaps the best way to use ADCP data is to couple it with more accurate turbulence data acquired over a smaller range. For example, hotwires could be used over a 2 m height range at mid-depth. This hotwire data could then be extrapolated over the entire channel using the ADCP data.

XI. Conclusions

In this paper, a comprehensive assessment has been made of the capability of an ADCP to capture turbulent flow structures of the lengthscales relevant to tidal turbine loading. The key conclusions are as follows:

1. Structures with wavelengths greater than 0.5m are likely to affect turbine loading. While the smallest of these can be predicted analytically, it is estimated that site-specific flow features will be generated at lengthscales from 1 m upwards so these lengthscales must be measured accurately during site surveys.
2. It has been shown that the ADCP acts as a low-pass filter to eddies. This filtering occurs first within each beam (intra-beam), before further alteration is caused by the combining of data from four spatial locations (inter-beam) and Doppler noise.
3. The main contributors to intra-beam filtering are:
   a. scattering particles failing to follow the flow fully.
   b. spatial averaging due to finite 'bin' size in both vertical and horizontal directions.
   c. averaging data from several 'pings' at different instants in time.

   Of these, spatial averaging tends to have the largest impact on the attenuation of high frequencies.
4. By combining the filters, it has been found that even optimistic calculations predict significant attenuation at lengthscales in the dangerous 1-35 m range. For a typical channel, information is attenuated by more than 90% for wavelengths below 4 m.
5. Intra-beam filtering means that some eddies will be completely attenuated while others are amplified, depending on the anisotropy and the phase difference between different components of each eddy. The overall effect of these filters is to skew the frequency spectrum between the real flow and the ADCP data.
6. While this low-pass filtering may alter some statistics by truncating the observed spectrum, it is most damaging when data is extracted for a few particular frequencies, as a turbine designer may do when assessing unsteady loading and fatigue life.
7. It is recommended that additional data is used to calibrate ADCP information. For example, hotwire data acquired over a small area can be used to examine which frequencies are incorrectly represented in the ADCP results.

References

[1] Winter, A.I. 2011. Differences in Fundamental Design Drivers for Wind and Tidal Turbines. Faculty of Engineering, Bristol.

[2] Milne, I.A., Sharma, R.N., Flay, R.G.J., & Bickerton, S. 2013. Characteristics of the turbulence in the flow at a tidal stream power site. Philosophical Transactions, The Royal Society.

[3] RDI. 1996. Acoustic Doppler Current Profiler, Principles of Operation, A Practical Primer.

[4] Lohrmann, A., Hackett, B., & Roed, L. P. 1990. High Resolution Measurements of Turbulence, Velocity and Stress Using a Pulse-to-Pulse Coherent Sonar. American Meteorological Society, 19-37.

[5] Nystrom, E. A., Oberg, K. A., & Rehmann, C. R. 2002. Measurement of Turbulence with Acoustic Doppler Current Profilers - Sources of Error and Laboratory Results: Proc Hydraulic Measurements and Experimental Methods Conference, Colorado.

[6] Theriault, K. B. 1986. Incoherent multibeam doppler current profiler performance: Part I - estimate variance. IEEE J. Oceanic Eng, 7-15.

[7] Theriault, K. B. 1986. Incoherent multibeam doppler current profiler performance: Part II - spatial response. IEEE J. Oceanic Eng, 16-25.

[8] Gargett, A. E., Tejada-Martinez, A. E., & E., Grosch C. 2008. Measuring turbulent large-eddy structures with an ADCP. Part 1: Vertical velocity variance. J. Marine Research, 66:155-189.

[9] Gargett, A. E., Tejada-Martinez, A. E., & E., Grosch C. 2009. Measuring turbulent large-eddy structures with an ADCP. Part 2: Horizontal velocity variance. J. Marine Research, 67:569-595.

[10] Togneri, M., & Masters, I. 2011. Parametrising Turbulent Marine Flows for a Blade Element Momentum Model of Tidal Stream Turbines. 9th European Wave and Tidal Energy Conference.

[11] Togneri, M., Masters, I., & Orme, J. 2011. Incorporating turbulent inflow conditions in a blade element momentum model of tidal stream turbines. Proceedings of the twenty-first International Offshore and Polar Engineering Conference, 757-762.

[12] Lueck, R. 2013. Measuring tidal channel turbulence with a Vertical Microstructure Profiler (VMP). Tech. rept. Rockland Scientific.

[13] Thomson, J., Polagye, B., Durgesh, V. & Richmond, M. C., 2012. Measurements of Turbulence at Two Tidal Energy Sites in Puget Sound, WA. IEEE J. Oceanic Eng. Vol. 37, No. 3. pp 363-374.

[14] Tchen, C. M. 1947. Mean value and correlation problems connected with the motion of small particles suspended in a turbulent fluid. Tech. rept. PhD, Delft.

[15] Hinze, J. O. 1975. Turbulence. McGraw-Hill.

[16] Melling, A., & Whilelaw, J.H. 1976. Principles and Practice of Laser-Doppler Anenometry. Academic Press.

[17] Hjelmfelt, & Mockros. 1965. Motion of Discrete Particles in a Turbulent Fluid. Applied Science, 149-161.

[18] Caruthers, J. W. 1977. Fundamentals of marine acoustics, p113-114. Elsevier.

[19] Taylor, G. I., 1938. The Spectrum of Turbulence. Proc. Royal Society, Series A. Vol. 164 No. 919. pp 476-490.

[20] Fung, J. C. H., Hunt, J. C. R., Malik, N. A., & Perkins, R. J. 1992. Kinematic simulation of homogeneous turbulence by unsteady random Fourier modes. J. Fluid Mechanics, 236:281-318.

[21] Favier, B., Godeferd, F. S., & Cambon, C. 2010. On space and time correlations of isotropic and rotating turbulence. Physics of Fluids, 22:015101.